Can acoustic and axionlike early dark energy still resolve the Hubble tension?

Théo Simon*

Laboratoire Univers and Particules de Montpellier (LUPM), CNRS and Université de Montpellier (UMR-5299), Place Eugène Bataillon, F-34095 Montpellier Cedex 05, France

(Received 2 November 2023; accepted 13 June 2024; published 22 July 2024)

In this paper, we reassess the ability of the acoustic early dark energy (ADE) and axionlike early dark energy (EDE) models to resolve the Hubble tension in light of the new Pantheon+ and SH_0ES data on the one hand, and the baryon oscillation spectroscopic survey (BOSS) luminous red galaxies (LRG) and extended baryon oscillation spectroscopic survey (eBOSS) quasistellar objects (QSO) data analyzed under the effective field theory of large-scale structures (EFTofLSS) on the other hand. We find that the Pantheon+ data, which favor a larger Ω_m value than the Pantheon data, have a strong constraining power on the ADE model, while the EFTofLSS analysis of the BOSS and eBOSS data only slightly increases the constraints. We establish that the ADE model is now strongly disfavored as a solution to the Hubble tension, with a remaining tension of 3.6σ (according to the Q_{DMAP} metric). In addition, we find that the axionlike EDE model performs better when confronted to the same datasets, with a residual tension of 2.5σ. This work shows that the Pantheon+ data can have a decisive impact on models which aim to resolve the Hubble tension.

DOI: 10.1103/PhysRevD.110.023528

I. INTRODUCTION

The Λ cold dark matter (ΛCDM) model provides a remarkable description of a wide variety of data from the early Universe, such as cosmic microwave background (CMB) or big bang nucleosynthesis, as well as observations of large-scale structure from the late Universe, including the baryon acoustic oscillation (BAO) and the uncalibrated luminosity distance to supernovae of type Ia. However, as the accuracy of cosmological observations has improved, the concordance cosmological model starts showing several experimental discrepancies. Among them, the Hubble tension refers to the inconsistency between local measurements of the current expansion rate of the Universe, quantified by the Hubble constant H_0, and the values inferred from early Universe data assuming the ΛCDM model. More precisely, this tension is essentially driven by the Planck Collaboration's observation of the CMB, which predicts a value of $H_0 = 67.27 \pm 0.60$ km/s/Mpc [1] within the ΛCDM model, and the value measured by the SH_0ES Collaboration using the Cepheid-calibrated cosmic distance ladder, whose latest measurement yields $H_0 = 73.04 \pm 1.04$ km/s/Mpc [2,3]. The disagreement between these observations results in an $\sim 5\sigma$ tension. Experimental efforts are under way to establish whether this discrepancy can be caused by systematic effects (see, e.g., [4–9]), but no definitive explanation has yet been found. This tension could therefore be indicative of new physics, most likely located in the prerecombination era, which involves a reduction in the sound horizon before recombination [10–15]. Early dark energy (EDE) models are capable of producing such an effect by increasing the total energy density of the Universe before recombination with the addition of a scalar field [16–37] (for review of EDE models, see Ref. [38], and for a review of models that could resolve the Hubble tension, see Refs. [15,39]). In the following, we consider the specific case of acoustic dark energy (ADE) developed in Refs. [40,41].

In this paper, we reassess the constraints on the ADE and axionlike EDE models (paying particular attention to the former) and their ability to resolve the Hubble tension, by successively evaluating the impact of the effective field theory (EFT) full-shape analysis applied to the baryon oscillation spectroscopic survey (BOSS) luminous red galaxies (LRG) [42] and extended baryon oscillation spectroscopic survey (eBOSS) quasistellar objects (QSO) [43] data, and the impact of the Pantheon+ data [44]. On the one hand, we make use of developments of the one-loop prediction of the galaxy power spectrum in redshift space from the effective field theory of large-scale structures (EFTofLSS)[1] applied to the BOSS [64] and eBOSS [65]

*Contact author: theo.simon@umontpellier.fr

[1]The first formulation of the EFTofLSS was carried out in Eulerian space in Refs. [45,46] and in Lagrangian space in [47]. Once this theoretical framework was established, many efforts were made to improve this theory and make it predictive, such as the understanding of renormalization [48,49], the IR resummation of the long displacement fields [50–55], and the computation of the two-loop matter power spectrum [56,57]. Then, this theory was developed in the framework of biased tracers (such as galaxies and quasars) in Refs. [58–63].

data in order to constrain the ADE and axionlike EDE models. This novel theoretical framework has made it possible to determine the ΛCDM parameters at precision higher than that from conventional BAO and redshift space distortions analyses, and even comparable to that of CMB experiments. In addition, the EFTofLSS provides an important consistency test for the ΛCDM model and its underlying assumptions, while allowing one to derive competitive constraints on models beyond ΛCDM (see, e.g., Refs. [64–83]). The study of the EFTofLSS impact on the ADE constraints is similar to what has already been done for the axionlike EDE model in Ref. [84] (see also Refs. [85–87]), which showed that this model leaves signatures in the galaxy power spectrum on large scales that can be probed by the BOSS data. On the other hand, we update the constraints on the ADE and axionlike EDE models by considering the Pantheon+ data from Ref. [44]. It has already been shown in Ref. [84] that the combination of the Pantheon+ data with a SH_0ES prior provides better constraints on the axionlike EDE model than the equivalent analysis including Pantheon data. This can be interpreted as a consequence of the fact that the Pantheon+ data prefer a value of $\Omega_m = 0.334 \pm 0.018$ which is higher than that of the Pantheon data. Together with the measured value of $H_0 = 100 \cdot h$ km/s/Mpc by SH_0ES, it leads to an increased value of $\omega_{\rm cdm} = \Omega_{\rm cdm} \cdot h^2$ (see Ref. [88]), which cannot be fully compensated by the presence of EDE, therefore degrading slightly the fit to CMB data.

In Sec. II, we provide a review of the ADE and axionlike EDE models, as well as a description of the analysis method and the datasets to which these models will be subjected. In Sec. III, we present the constraints of the ADE model and compare them to the axionlike EDE case, while in Sec. IV we consider some additional variations of the model under study.

II. THE MODEL AND THE DATA

A. Review of the ADE model

In this paper, we focus on the ADE model proposed in Ref. [40] (see Ref. [38] for a general introduction). In this model, the ADE equation-of-state parameter $w_{\rm ADE}(a) = P_{\rm ADE}(a)/\rho_{\rm ADE}(a)$ is modeled as

$$w_{\rm ADE}(a) = \frac{1 + w_f}{[1 + (a_c/a)^{3(1+w_f)/p}]^p} - 1. \tag{1}$$

In Fig. 1, we plot the evolution of $w_{\rm ADE}$ as a function of the cosmological redshift z. This figure clearly illustrates that in this model the critical redshift $z_c = (a_0 - a_c)/a_c$ sets a transition in the ADE equation of state from $w_{\rm ADE} \to -1$, when $z \gg z_c$, to $w_{\rm ADE} \to w_f$, when $z \ll z_c$. Therefore, this parametrization allows the ADE component to behave in a similar way to dark energy before the critical redshift (exactly like the axionlike EDE model), while it allows the late-time value of the ADE equation of state to be set thanks to the parameter w_f. As shown in Fig. 1, the rapidity of this transition is controlled by the parameter p, which is set at $p = 1$ for our baseline model, corresponding to the modeling of the time-averaged background equation-of-state of the axionlike EDE model [89]. Similar to the axionlike EDE case where $w_{\rm EDE}(z \ll z_c) = 1/2$ (see below), the ADE dilutes faster than the radiation (i.e., $w_f > w_r$) below the critical redshift, in order to suppress the contribution of this component to the total budget of the Universe at the moment of the CMB.

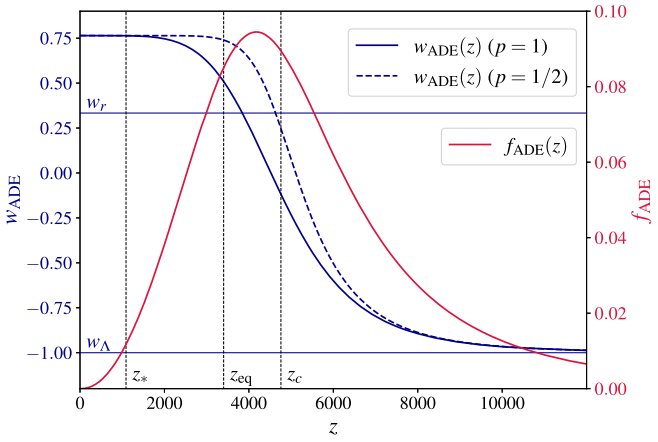

FIG. 1. Evolution of the ADE equation-of-state parameter $w_{\rm ADE}$ as well as the ADE fractional energy density $f_{\rm ADE}(z_c)$ as a function of the cosmological redshift z. To perform this plot, we use the best-fit values of the BAO/$f\sigma_8$ + Pan + M_b analysis (see Table I). For the ADE equation-of-state parameter, we set $p = 1$, which corresponds to our baseline setup, and $p = 1/2$, which corresponds to the setup of Ref. [40]. The horizontal lines correspond to the radiation and dark energy equation-of-state parameters w_r and w_Λ, respectively, while the dashed vertical lines correspond to the redshift of recombination z_*, the redshift of the matter-radiation equality $z_{\rm eq}$, and the ADE critical redshift z_c.

Let us note that the parametrization of Eq. (1) can be achieved in the K-essence class of dark energy models. In particular, the dark component is here a perfect fluid represented by a minimally coupled scalar field ϕ with a general kinetic term [90]. For the specific case of a constant sound speed c_s^2, the Lagrangian density is written as [91]

$$P(X, \phi) = \left(\frac{X}{A}\right)^{\frac{1-c_s^2}{2c_s^2}} X - V(\phi), \tag{2}$$

where $X = -\nabla^2\phi/2$ and A is a constant density scale [40]. In this category of models, $w_{\rm ADE} \to c_s^2$ if the kinetic term dominates, whereas $w_{\rm ADE} \to -1$ if the potential $V(\phi)$ dominates. The main advantage of the ADE model over the axionlike EDE model is that the former provides a general class of exact solutions, while the latter requires a specific set of initial conditions to achieve a similar phenomenology [40].

Since the ADE equation-of-state parameter changes over time, the conservation equation gives

$$\rho_{\rm ADE}(a) = \rho_{\rm ADE,0} e^{3\int_a^1 [1+w_{\rm ADE}(a')]da'/a'}, \tag{3}$$

which allows us to define the ADE fractional energy density as

$$f_{\rm ADE}(a) = \frac{\rho_{\rm ADE}(a)}{\rho_{\rm tot}(a)}. \tag{4}$$

In Fig. 1, we also plot the evolution of $f_{\rm ADE}$ as a function of the cosmological redshift z. We notice that this parameter is maximal around the ADE equation-of-state transition, set by the critical redshift z_c, namely, when $f_{\rm ADE}(z \sim z_c)$. Then, this parameter becomes subdominant at the time of recombination, with $f_{\rm ADE}(z_*) \sim 1\%$ [92].

Finally, the ADE model we are considering is described by the three following parameters:

$$\{z_c, f_{\rm ADE}(z_c), w_f\}. \tag{5}$$

Reference [40] also considers the variation of a fourth parameter that determines the behavior of the ADE perturbations, namely, their rest frame sound speed $c_s^2(k,a)$. Unlike the standard axionlike EDE model (see below), we assume for this model the scale independence of this parameter, i.e., $c_s^2(k,a) = c_s^2(a)$, which is equivalent to assuming a perfect fluid with a linear dispersion relation. In addition, because of the sharp transition of the $w_{\rm ADE}$ parameter, the impact of the ADE component on the perturbed universe is localized in time, which implies that we can approximate this parameter as a constant. Thus, Ref. [40] varies this parameter to its critical redshift value, namely, $c_s^2 = c_s^2(a = a_c)$, in addition to the three other parameters listed above. In our baseline model, we consider that $c_s^2 = w_f$, insofar as it has been shown to be a good approximation near the best fit [40]. However, in Sec. IV, we consider two model variations of our baseline model: (i) the c_s^2ADE model, where we free these two parameters independently, and (ii) the cADE model, where we set $c_s^2 = w_f = 1$. Let us note that there exists a second difference between Refs. [40,41] and our baseline analysis, since these references set $p = 1/2$, which leads to a sharper transition than ours (with $p = 1$), as shown in Fig. 1. However, the impact of this parameter on cosmological results is very minor, and we have verified that we obtain the same results as Ref. [41] with $p = 1$.

B. Review of the axionlike EDE model

For comparison, we also consider the axionlike EDE model [16–18], which corresponds to an extension of the ΛCDM model, where the existence of an additional subdominant oscillating scalar field ϕ is considered. The EDE field dynamics is described by the Klein-Gordon equation of motion (at the homogeneous level),

$$\ddot{\phi} + 3H\dot{\phi} + V_{n,\phi}(\phi) = 0, \tag{6}$$

where $V_n(\phi)$ is a modified axionlike potential defined as

$$V_n(\phi) = m^2 f^2 [1 - \cos(\phi/f)]^n. \tag{7}$$

f and m correspond to the decay constant and the effective mass of the scalar field, respectively, while the parameter n controls the rate of dilution after the field becomes dynamical. In the following, we will use the redefined field quantity $\Theta = \phi/f$ for convenience, such that $-\pi \leq \Theta \leq +\pi$. At early times, when $H \gg m$, the scalar field ϕ is frozen at its initial value since the Hubble friction prevails, which implies that the EDE behaves like a form of dark energy and that its contribution to the total energy density increases relative to the other components. When the Hubble parameter drops below a critical value ($H \sim m$), the field starts evolving toward the minimum of the potential and becomes dynamical. The EDE contribution to the total budget of the Universe is maximum around a critical redshift z_c, after which the energy density starts to dilute with an equation-of-state parameter $w_{\rm EDE}(a)$ approximated by [89,93]

$$w_{\rm EDE} = \begin{cases} -1 & \text{if } z > z_c, \\ \frac{n-1}{n+1} & \text{if } z < z_c. \end{cases} \tag{8}$$

In the following, we will fix $n = 3$ as it was found that the data were relatively insensitive to this parameter provided $2 \lesssim n \lesssim 5$ [18], implying that in this specific model $w_{\rm EDE}(z \ll z_c) = 1/2$. Instead of the theory parameters f and m, we make use of z_c and $f_{\rm EDE}(z_c)$ determined through a shooting method [18]. We also include the initial field value Θ_i as a free parameter, whose main role once $f_{\rm EDE}(z_c)$ and z_c are fixed is to set the dynamics of perturbations right around z_c through the EDE sound speed c_s^2. Finally, the axionlike EDE model is described by the three following parameters:

$$\{z_c, f_{\rm EDE}(z_c), \Theta_i\}. \tag{9}$$

Let us note that the axionlike EDE sound speed $c_s^2(a,k) = \delta P_{\rm EDE}(k,a)/\delta\rho_{\rm EDE}(k,a)$ is scale and time dependent, and is entirely determined by the three EDE parameters specified above. In the fluid approximation, one can estimate the a and k dependencies of this parameter as [17,89]

$$c_s^2(a,k) = \begin{cases} 1, & a \leq a_c, \\ \frac{2a^2(n-1)\varpi^2(a)+k^2}{2a^2(n+1)\varpi^2(a)+k^2}, & a > a_c, \end{cases} \tag{10}$$

where ϖ corresponds to the angular frequency of the oscillating background field, which has a time dependency fixed by z_c, n, and Θ_i (see Ref. [89]). Let us note however that the axionlike EDE model we consider in this paper does not rely on this fluid approximation, and instead

solves the exact (linearized) Klein-Gordon equation, which is expressed in synchronous gauge as [94]

$$\delta\phi_k'' + 2H\delta\phi_k' + [k^2 + a^2 V_{n,\phi\phi}]\delta\phi_k = -h'\phi'/2, \quad (11)$$

where the prime denotes derivatives with respect to conformal time.

C. Data and analysis methods

We perform Markov chain Monte Carlo (MCMC) analyses, confronting the ADE model with recent cosmological observations. To do so, we make use of the Metropolis-Hastings algorithm from the MontePython-v3[2] code [95,96] interfaced with our modified CLASS [97,98] version.[3] In this paper, we perform various analyses from a combination of the following datasets:

(i) *Planck*: The low-ℓCMB temperature and polarization autocorrelations (TT, EE), and the high-ℓTT, TE, EE data [99], as well as the gravitational lensing potential reconstruction from *Planck* 2018 [100].
(ii) ext-BAO: The low-z BAO data gathered from the 6-degree Field Galaxy Survey at $z = 0.106$ [101], Sloan Digital Sky Survey Data Release 7 at $z = 0.15$ [102].
(iii) BOSS BAO/$f\sigma_8$: BAO measurements cross-correlated with the redshift space distortion measurements from the CMASS and LOWZ galaxy samples of BOSS DR12 LRG at $z = 0.38$, 0.51, and 0.61 [42].
(iv) eBOSS BAO/$f\sigma_8$: BAO measurements cross-correlated with the redshift space distortion measurements from the CMASS and LOWZ quasar samples of eBOSS DR16 QSO at $z = 1.48$ [43].
(v) EFTofBOSS: The EFTofLSS analysis of BOSS DR12 LRG cross-correlated with the reconstructed BAO parameters [103]. The SDSS-III BOSS DR12 galaxy sample data and covariances are described in [42,104]. The measurements obtained in [73] are from BOSS catalogs DR12 (v5) combined CMASS-LOWZ [105], and are divided in redshift bins LOWZ $0.2 < z < 0.43$ ($z_{\rm eff} = 0.32$), and CMASS $0.43 < z < 0.7$ ($z_{\rm eff} = 0.57$), with north and south galactic skies for each, respectively, denoted NGC and SGC. From these data, we use the monopole and quadrupole moments of the galaxy power spectrum. The theory prediction and likelihood for the full-modeling information are made available through PyBird [68], together with the West-coast parametrization [71,83,106] as implemented in Ref. [68]. In our analyses, we vary seven EFT parameters per sky cut, namely, three bias parameters [b_1, b_3, and $c_2 \equiv (b_2 + b_4)/\sqrt{2}$], two counterterm parameters ($c_{\rm ct}$ and $c_{r,1}$), and two stochastic parameters ($c_{\epsilon,0}$ and $c_\epsilon^{\rm quad}$). The physical meaning of these parameters and the priors used are described in detail in Ref. [83]. Finally, we analyze the BOSS data up to $k_{\rm max}^{\rm CMASS} = 0.23h$ Mpc^{-1} for the CMASS sky cut and up to $k_{\rm max}^{\rm LOWZ} = 0.20h$ Mpc^{-1} for the LOWZ sky cut (as determined in Ref. [67]).
(vi) EFTofeBOSS: The EFTofLSS analysis [65] of eBOSS DR16 QSOs [43]. The QSO catalogs are described in [107], and the covariances are built from the effective EZ-mocks described in [108]. There are about 343 708 quasars selected in the redshift range $0.8 < z < 2.2$, with $z_{\rm eff} = 1.52$ divided into two skies, NGC and SGC [109,110]. From these data, we use the monopole and quadrupole moments of the galaxy power spectrum. The theory prediction and likelihood for the full-modeling information are made available through PyBird, together with the West-coast parametrization as implemented in Ref. [65]. We use the same EFT parameters as for EFTofBOSS, and we set $k_{\rm max}^{\rm eBOSS} = 0.24h$ Mpc^{-1} (as determined in Ref. [65]).
(vii) Pantheon: The Pantheon catalog of uncalibrated luminosity distance of type-Ia supernovae (SNeIa) in the range $0.01 < z < 2.3$ [111].
(viii) Pantheon+: The newer Pantheon+ catalog of uncalibrated luminosity distance of SNeIa in the range $0.001 < z < 2.26$ [44].
(ix) Pantheon + /S$\boldsymbol{H}_0$ES: The Pantheon+ catalog cross-correlated with the absolute calibration of the SNeIa from SH_0ES [2].
(x) M_b: Gaussian prior from the most up-to-date late-time measurement of the absolute calibration of the SNeIa from SH_0ES, $M_b = -19.253 \pm 0.027$ [2] corresponding to $H_0 = (73.04 \pm 1.04)$ km/s/Mpc.

We choose *Planck*+ext-BAO + BOSS BAO/$f\sigma_8$+ eBOSS BAO/$f\sigma_8$ + Pantheon (optionally with the M_b prior) as our baseline analysis, called, for the sake of simplicity, "BAO/$f\sigma_8$ + Pan." In order to assess the impact of the EFT full-shape analysis of the BOSS and eBOSS data on the ADE resolution of the Hubble tension, we compare the baseline analysis with an equivalent analysis that includes the EFTofBOSS and EFTofeBOSS likelihoods instead of the BOSS and eBOSS BAO/$f\sigma_8$ likelihoods. This analysis is called "EFT + Pan." Finally, in order to gauge the influence of the new Pantheon data, we replace the Pantheon likelihood with the Pantheon+ likelihood. This analysis referred to as "EFT + PanPlus" is compared with the aforementioned EFTofLSS analysis. In Appendix A, we show explicitly that the addition of the M_b prior on top of the Pantheon+ likelihood is equivalent to the use of the full "Pantheon + /SH_0ES" likelihood as provided in Ref. [2].

For all runs performed, we impose large flat priors on $\{\omega_b, \omega_{\rm cdm}, H_0, A_s, n_s, \tau_{\rm reio}\}$, which correspond,

[2]https://github.com/brinckmann/montepython_public.
[3]https://github.com/PoulinV/AxiCLASS.

respectively, to the dimensionless baryon energy density, the dimensionless cold dark matter energy density, the Hubble parameter today, the variance of curvature perturbations centered on the pivot scale $k_p = 0.05\ \mathrm{Mpc}^{-1}$ (according to the *Planck* convention), the scalar spectral index, and the reionization optical depth. Regarding the free parameters of the ADE model, we impose logarithmic flat priors on z_c, and flat priors on $f_{\mathrm{ADE}}(z_c)$ and w_{ADE},

$$\begin{aligned} 3 &\leq \log_{10}(z_c) \leq 4.5, \\ 0 &\leq f_{\mathrm{ADE}}(z_c) \leq 0.2, \\ 0 &\leq w_f \leq 3.6. \end{aligned}$$

Note that we have verified that a wider prior on w_f does not impact our results. When we compare the ADE model with the axionlike EDE model, we use the following priors for the latter:

$$\begin{aligned} 3 &\leq \log_{10}(z_c) \leq 4, \\ 0 &\leq f_{\mathrm{EDE}}(z_c) \leq 0.5, \\ 0 &\leq \Theta_i \leq \pi. \end{aligned}$$

In this paper, we use *Planck* conventions for the treatment of neutrinos; that is, we include two massless and one massive species with $m_\nu = 0.06$ eV [1]. In addition, we use HMcode [112] to estimate the nonlinear matter clustering solely for the purpose of the CMB lensing. We define our MCMC chains to be converged when the Gelman-Rubin criterion $R - 1 < 0.05$. Finally, we extract the best-fit parameters from the procedure highlighted in the Appendix of Ref. [15], and we produce our figures thanks to GetDist [113].

In this paper, we compare the models with each other using two main metrics. First, in order to assess the ability of an extended model $\mathcal{M}$ to fit all the cosmological data, we compute the Akaike information criterion (AIC) of this model relative to that of the ΛCDM. This metric is defined as follows:

$$\Delta\mathrm{AIC} = \chi^2_{\mathrm{min},\mathcal{M}} - \chi^2_{\mathrm{min},\Lambda\mathrm{CDM}} + 2\cdot(N_{\mathcal{M}} - N_{\Lambda\mathrm{CDM}}), \quad (12)$$

where $\mathcal{M} \in \{\mathrm{ADE}, \mathrm{EDE}, c_s^2\mathrm{ADE}, \mathrm{cADE}\}$, and where $N_{\mathcal{M}}$ stands for the number of free parameters of the model. This metric enables us to determine whether the fit within a particular model $\mathcal{M}$ significantly improves that of ΛCDM by penalizing models with a larger number of degrees of freedom. Second, in order to gauge the ability of the extended model $\mathcal{M}$ to solve the Hubble tension for a given combination of data $\mathcal{D}$ (which does not include the M_b prior), we also compute the residual Hubble tension thanks to the difference of the maximum *a posteriori* (DMAP) [114] determined by

$$Q_{\mathrm{DMAP}} = \sqrt{\chi^2_{\mathrm{min},\mathcal{M}}(\mathcal{D}+M_b) - \chi^2_{\mathrm{min},\mathcal{M}}(\mathcal{D})}. \quad (13)$$

This metric allows us to determine how the addition of the M_b prior to the dataset $\mathcal{D}$ impacts the fit within a particular model $\mathcal{M}$. Reference [15] asserts that a model is a good candidate for solving the Hubble tension if it meets these two conditions: $\Delta AIC < -6.91$ and $Q_{\mathrm{DMAP}} < 3\sigma$. Finally, we also consider the Gaussian tension (GT) computed as

$$\mathrm{GT} = \frac{\overline{H_0}(\mathrm{SH_0ES}) - \overline{\mathrm{H_0}}(\mathcal{D})}{\sqrt{\sigma^2_{H_0}(\mathrm{SH_0ES}) + \sigma^2_{H_0}(\mathcal{D})}}, \quad (14)$$

where $\overline{H_0}$ and σ_{H_0} correspond to the mean and standard deviation of the Hubble parameter today determined from the SH_0ES experiment and the dataset $\mathcal{D}$ (within the model $\mathcal{M}$). The Gaussian tension is certainly the most direct metric for quantifying the Hubble tension, but the main problem with this metric is that it is unable to favor a complex model in which some parameters become irrelevant in the ΛCDM limit. If a probability density function deviates from Gaussian in a complex model (as is the case for EDE models), only the Gaussian ΛCDM limit has significant statistical weight [15,86].

III. COSMOLOGICAL RESULTS

In this section, we discuss the cosmological constraints of the ADE and axionlike EDE models and their ability to solve the Hubble tension by successively evaluating the impact of the EFT full-shape analysis of the BOSS and eBOSS data (compared with the standard BAO/$f\sigma_8$ analysis) and the impact of the new Pantheon data (compared with the equivalent older data) on these models. The cosmological constraints for the ADE model are shown in Table I, while the χ^2_{min} values associated with each likelihood are presented in Table III of Appendix B. In Table I, we also display the $\Delta\chi^2_{\mathrm{min}}$ and the associated ΔAIC with respect to ΛCDM, as well as the Q_{DMAP} for several combinations of data.

Our baseline combination of data denoted BAO/$f\sigma_8$ + Pan refers to *Planck*+ext-BAO + BOSS BAO/$f\sigma_8$ + eBOSS BAO/$f\sigma_8$ + Pantheon corresponding roughly to that used in Ref. [41].[4] For this analysis, combined with the M_b prior, we find $f_{\mathrm{ADE}}(z_c) = 0.081 \pm 0.018$ and $H_0 = 71.24 \pm 0.68$ km/s/Mpc for the ADE model, leading to a residual Hubble tension of $Q_{\mathrm{DMAP}} = 2.6\sigma$ and a preference over ΛCDM of $\Delta\mathrm{AIC} = -22.3$ (see Table I). Note that this χ^2 improvement is mainly driven by the SH_0ES data (as is also the case in the remainder of this paper), implying that

[4]Note that this analysis used another SH_0ES prior, $H_0 = 74.03 \pm 1.42$ km/s/Mpc, from Ref. [115], and does not take into account the redshift space distortion information (but only the BAO).

TABLE I. Mean (best fit) $\pm 1\sigma$ (or 2σ for one-sided bounds) of reconstructed parameters in the ADE model confronted to various datasets. All datasets include *Planck* + ext-BAO data, while we consider either the BAO/$f\sigma_8$ information or the EFT full-shape analysis for the BOSS and eBOSS data, and we consider either the Pantheon data or the Pantheon+ data (with and without the M_b prior). We also display for all datasets the $\Delta\chi^2_{\rm min}$ with respect to ΛCDM, the associated ΔAIC, as well as the $Q_{\rm DMAP}$. Finally, $Q_{\rm DMAP}(\Lambda{\rm CDM})$ and $Q_{\rm DMAP}({\rm EDE})$ correspond to the $Q_{\rm DMAP}$ of the ΛCDM and axionlike EDE models for the equivalent datasets.

	BAO/$f\sigma_8$ + Pan		EFT + Pan		EFT + PanPlus	
M_b prior?	No	Yes	No	Yes	No	Yes
$f_{\rm ADE}(z_c)$	$< 0.060(0.034)$	$0.081(0.090) \pm 0.018$	$< 0.049(0.010)$	$0.068(0.076) \pm 0.019$	$< 0.036(0.011)$	$0.073(0.082) \pm 0.020$
$\log_{10}(z_c)$	*Unconstrained* (3.748)	$3.655(3.677) \pm 0.093$	*Unconstrained* (3.713)	$3.676(3.686)^{+0.095}_{-0.120}$	*Unconstrained* (3.957)	$3.692(3.724)^{+0.098}_{-0.120}$
w_f	$> 0.49(0.69)$	$0.79(0.76)^{+0.10}_{-0.12}$	$> 0.59(0.70)$	$0.78(0.75)^{+0.11}_{-0.13}$	$> 0.61(0.57)$	$0.76(0.73) \pm 0.13$
H_0	$68.44(69.04)^{+0.47}_{-0.93}$	$71.24(71.49) \pm 0.68$	$68.16(68.26)^{+0.41}_{-0.53}$	$71.01(71.31) \pm 0.73$	$68.03(68.16)^{+0.43}_{-0.53}$	$71.13(71.29) \pm 0.73$
$\omega_{\rm cdm}$	$0.1212(0.1239)^{+0.0012}_{-0.0030}$	$0.1291(0.1305) \pm 0.0027$	$0.1196(0.1202)^{+0.0009}_{-0.0015}$	$0.1267(0.1280) \pm 0.0027$	$0.1201(0.1211)^{+0.0011}_{-0.0015}$	$0.1278(0.1294) \pm 0.0028$
$10^2\omega_b$	$2.259(2.269)^{+0.016}_{-0.023}$	$2.304(2.309) \pm 0.021$	$2.254(2.252)^{+0.014}_{-0.017}$	$2.303(2.306) \pm 0.022$	$2.250(2.258) \pm 0.018$	$2.306(2.311) \pm 0.022$
$10^9 A_s$	$2.123(2.119) \pm 0.030$	$2.159(2.152) \pm 0.031$	$2.111(2.111) \pm 0.030$	$2.148(2.151)^{+0.028}_{-0.032}$	$2.111(2.116)^{+0.028}_{-0.036}$	$2.151(2.150)^{+0.028}_{-0.033}$
n_s	$0.9711(0.9748)^{+0.0041}_{-0.0074}$	$0.9900(0.9925) \pm 0.0061$	$0.9684(0.9686)^{+0.0040}_{-0.0048}$	$0.9878(0.9904) \pm 0.0060$	$0.9679(0.9697)^{+0.0038}_{-0.0047}$	$0.9890(0.9906) \pm 0.0063$
$\tau_{\rm reio}$	$0.0583(0.0540)^{+0.0063}_{-0.0075}$	$0.0588(0.0561)^{+0.0066}_{-0.0077}$	$0.0572(0.0573) \pm 0.0070$	$0.0590(0.0584)^{+0.0067}_{-0.0077}$	$0.0570(0.0574) \pm 0.0072$	$0.0585(0.0573)^{+0.0065}_{-0.0077}$
S_8	$0.828(0.834)^{+0.011}_{-0.013}$	$0.843(0.846) \pm 0.013$	$0.820(0.823) \pm 0.010$	$0.832(0.835) \pm 0.012$	$0.825(0.830)^{+0.010}_{-0.011}$	$0.836(0.842) \pm 0.013$
Ω_m	$0.3083(0.3089) \pm 0.0054$	$0.3011(0.3018) \pm 0.0050$	$0.3074(0.3078) \pm 0.0050$	$0.2983(0.2983) \pm 0.0047$	$0.3096(0.3107)^{+0.0047}_{-0.0053}$	$0.2994(0.3014) \pm 0.0047$
$\Delta\chi^2_{\rm min}$	-3.9	-28.3	-1.4	-24.9	-1.3	-27.8
ΔAIC	$+2.1$	-22.3	$+4.6$	-18.9	$+4.7$	-21.8
$Q_{\rm DMAP}$	2.6σ		2.9σ		3.6σ	
$Q_{\rm DMAP}({\rm EDE})$	1.5σ		2.4σ		2.5σ	
$Q_{\rm DMAP}(\Lambda{\rm CDM})$	5.6σ		5.6σ		6.3σ	

this preference over ΛCDM will no longer be significant if the Hubble tension is due to a systematic error in the data. Let us underline that with our baseline combination of data, the ADE model satisfies both Ref. [15] conditions. In addition, we find for the ADE model that GT $= 3.7\sigma$ for our original combination of data. We are now assessing how the EFTofLSS on the one hand, and the new data from Pantheon+, on the other hand, change these conclusions.

A. Impact of the EFTofLSS analysis

In the top panel of Fig. 2, we show the reconstructed 2D posteriors of the ADE model for the analysis with the BOSS and eBOSS BAO/$f\sigma_8$ likelihoods (namely, the BAO/$f\sigma_8$ + Pan analysis), as well as for the analysis with the EFTofBOSS and EFTofeBOSS likelihoods (namely, the EFT + Pan analysis), either with or without the M_b prior. To isolate the effect of the EFT full-shape analysis, we carry out these analyses using only the older Pantheon data.

For the analyses without the M_b prior, the addition of the EFT likelihood has a non-negligible impact on the $f_{\rm ADE}(z_c)$, w_f, and H_0 constraints. The upper bound of the ADE fractional energy density and the lower bound of w_f are indeed both improved by ∼20%, while the standard deviation of H_0 is reduced by ∼35%.

When we consider the M_b prior, EFTofBOSS and EFTofeBOSS do not improve the parameter constraints of this model over the BAO/$f\sigma_8$ information. However, these likelihoods shift $f_{\rm ADE}(z_c)$ and H_0 toward smaller values of 0.7σ and 0.3σ,[5] respectively. The EFT full-shape analysis of the BOSS and eBOSS data therefore slightly reduces the ability of this model to resolve the Hubble tension, and the $Q_{\rm DMAP}$ changes from 2.6σ to 2.9σ when EFT likelihoods are considered (see Table I). In particular, the $\chi^2_{\rm min}$ associated with the M_b prior is degraded by 1.0 compared to the BAO/$f\sigma_8$ analysis. In addition, the preference for this model over the ΛCDM model is slightly reduced, given that the ΔAIC changes from −22.3 to −18.9 when the EFT likelihood is added (see Table I). Note that at this point, the ADE model still satisfies both conditions of Ref. [15], even though $Q_{\rm DMAP} \sim 3\sigma$. However, the Gaussian tension changes from 3.7σ to 4.3σ when EFT likelihoods are considered, which can be explained by the fact that the $f_{\rm ADE}(z_c)$ parameter is better constrained by the EFT + Pan dataset.

For the axionlike EDE case, we find for the equivalent analyses (see Table III of Appendix B) that the $Q_{\rm DMAP}$ changes from 1.5σ to 2.4σ, and that the ΔAIC changes from −29.1 to −22.9, when EFT likelihoods are added.[6] The ADE model slightly better supports the addition of the EFT likelihood compared to the EDE model, insofar as the $Q_{\rm DMAP}$ and ΔAIC are more stable (see Table I). However, the EDE model remains a better model to solve the Hubble tension, with $Q_{\rm DMAP} = 2.4\sigma$ for the EFT + Pan analysis, compared to $Q_{\rm DMAP} = 2.9\sigma$ for the ADE model, and has a better fit to the data when the M_b prior is added, with ΔAIC $= -22.9$ compared to ΔAIC $= -18.9$ for the ADE model. For a detailed discussion of the EFTofLSS impact on the EDE model in the framework of the BOSS data, please refer to Ref. [84].[7]

B. Impact of the Pantheon+ data

Let us now turn to the impact of the latest Pantheon data, namely, the Pantheon+ data, on the ability of these models to resolve the Hubble tension. In the bottom panel of Fig. 2, we show the reconstructed 2D posteriors of the ADE model for the analyses with the old Pantheon data (i.e., the EFT + Pan analysis), as well as for the analyses with the updated data (i.e., the EFT + PanPlus analysis). To isolate the effect of the Pantheon+ data, we carry out these analyses using only the EFT full-shape analysis of the BOSS and eBOSS data.

The analysis with the Pantheon+ data, but without any SH_0ES prior, improves significantly the 95% C.L. constraints on $f_{\rm ADE}(z_c)$ by ∼30%. This implies that H_0 is shifted down by 0.2σ[8] compared to the analysis with the old Pantheon data. Although the ADE model prefers a higher value of $\omega_{\rm cdm}$ than ΛCDM (because ADE slows down the evolution of the growing modes), the larger Ω_m favored by the Pantheon+ data ($\Omega_m = 0.334 \pm 0.018$ [44]) leads to a large $\omega_{\rm cdm} = \Omega_{\rm cdm} \cdot h^2$, which is not sufficiently compensated for by ADE. Then, to offset the high value of Ω_m, the current Hubble parameter decreases slightly, as well as $f_{\rm ADE}(z_c)$, since the latter is positively correlated with H_0.

When the M_b prior is included, nonzero contributions of ADE are favored. One may have expected that the tighter

[5]Since we are considering here the same experiments (with different methods for extracting cosmological constraints), we use the following metric: $2 \cdot (\theta_i - \theta_j)/(\sigma_{\theta,i} + \sigma_{\theta,j})$, where θ_i and $\sigma_{\theta,i}$ are, respectively, the mean value and the standard deviation of the parameter θ for the dataset i.

[6]The similar analysis in Ref. [84], which does not include the eBOSS data, determined that $Q_{\rm DMAP} = 2.0\sigma$ for the BAO/$f\sigma_8$ + Pan analysis and that $Q_{\rm DMAP} = 2.1\sigma$ for the EFT + Pan analysis (see Table 8 in Ref. [84]). This difference is due solely to the eBOSS data: The χ^2 of the eBOSS BAO/$f\sigma_8$ likelihood is improved when the M_b prior is added (which decreases the $Q_{\rm DMAP}$ of the BAO/$f\sigma_8$ + Pan analysis), while the χ^2 is degraded for the EFTofeBOSS likelihood when the M_b prior is added (which increases the $Q_{\rm DMAP}$ of the EFT + Pan analysis).

[7]Note that Ref [84] used an H_0 prior equivalent to the M_b prior and did not consider the EFTofeBOSS likelihood (as well as the eBOSS BAO/$f\sigma_8$ likelihood). We leave a detailed evaluation of the impact of eBOSS data on the EDE model for future work.

[8]Since we are considering here different experiments, we use the following metric: $(\theta_i - \theta_j)/\sqrt{\sigma^2_{\theta,i} + \sigma^2_{\theta,j}}$, where θ_i and $\sigma_{\theta,i}$ are, respectively, the mean value and the standard deviation of the parameter θ for the dataset i.

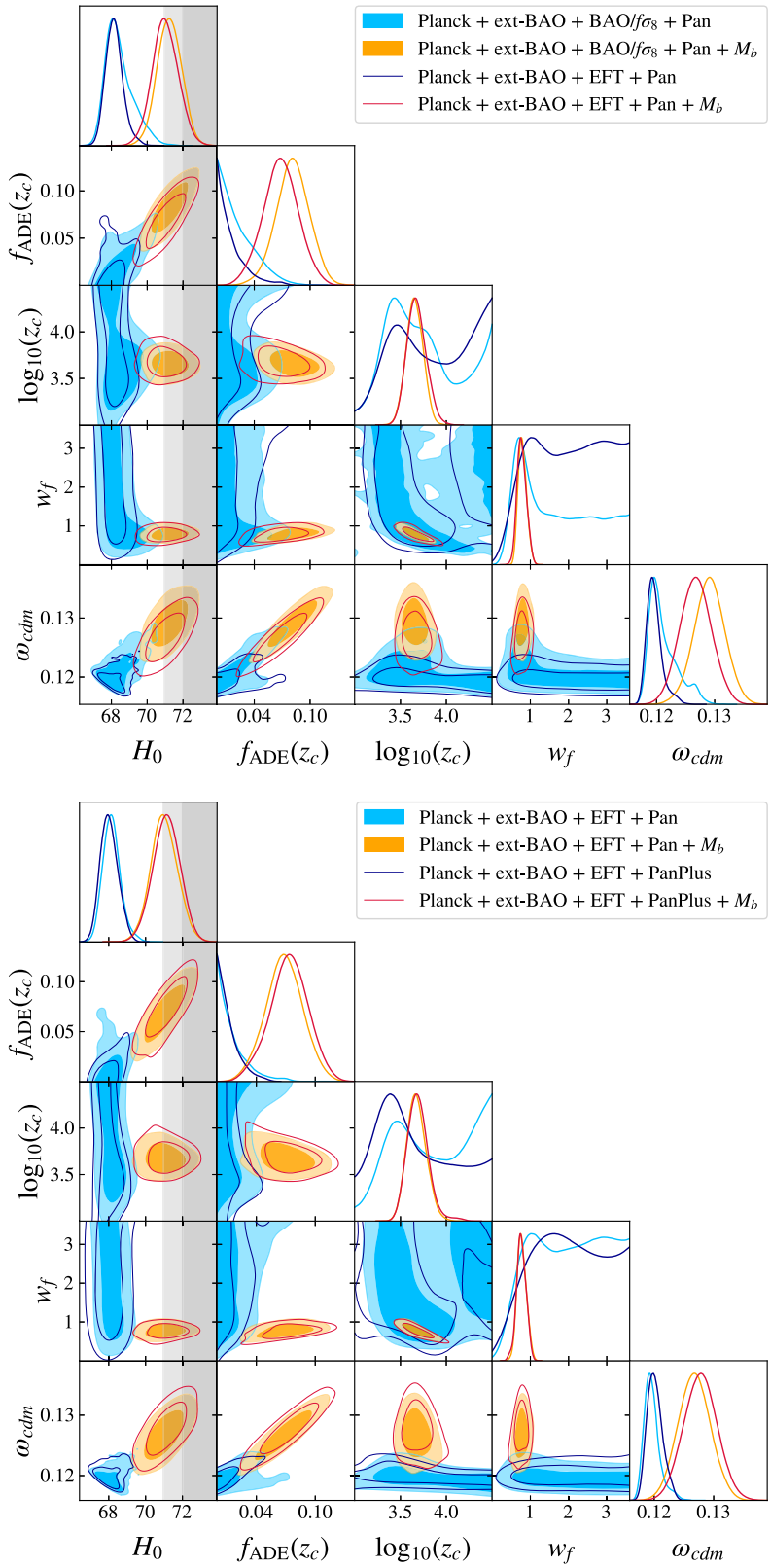

FIG. 2. Top panel: 2D posterior distributions reconstructed from the BAO/$f\sigma_8$ + Pan dataset compared with the 2D posterior distributions reconstructed from the EFT + Pan dataset, either with or without the M_b prior. Bottom panel: 2D posterior distributions reconstructed from the EFT + Pan dataset compared with the 2D posterior distributions reconstructed from the EFT + PanPlus dataset, either with or without the M_b prior. The gray bands correspond to the H_0 constraint associated with the M_b prior $H_0 = (73.04 \pm 1.04)$ km/s/Mpc [2].

TABLE II. Mean (best fit) $\pm 1\sigma$ (or 2σ for one-sided bounds) of reconstructed parameters in the EDE, c_s^2ADE, and cADE models confronted to the $Planck$ + ext-BAO + EFT + PanPlus + M_b dataset, i.e., the most up-to-date dataset. We also display for each model the $\Delta\chi^2_{\rm min}$ with respect to ΛCDM, the associated ΔAIC, as well as the $Q_{\rm DMAP}$.

	EDE	c_s^2ADE	cADE
$f_{\rm ADE/EDE}(z_c)$	$0.116(0.128)^{+0.023}_{-0.021}$	$0.103(0.080)^{+0.028}_{-0.046}$	$0.079(0.087) \pm 0.019$
$\log_{10}(z_c)$	$3.69(3.84)^{+0.20}_{-0.16}$	$3.61(3.73)^{+0.12}_{-0.10}$	$3.540(3.532) \pm 0.058$
Θ_i	$2.77(2.88)^{+0.15}_{-0.072}$	⋯	⋯
w_f	⋯	*Unconstrained* (0.71)	⋯
c_s^2	⋯	$> 0.701(0.72)$	⋯
H_0	$71.67(71.84) \pm 0.77$	$70.76(71.23) \pm 0.70$	$70.95(71.23) \pm 0.73$
$\omega_{\rm cdm}$	$0.1303(0.1309) \pm 0.0030$	$0.1257(0.1294) \pm 0.0024$	$0.1273(0.1286) \pm 0.0028$
$10^2\omega_b$	$2.294(2.312) \pm 0.024$	$2.304(2.310) \pm 0.020$	$2.305(2.308) \pm 0.021$
$10^9 A_s$	$2.149(2.143)^{+0.027}_{-0.034}$	$2.152(2.150)^{+0.030}_{-0.036}$	$2.149(2.158) \pm 0.031$
n_s	$0.9898(0.9951) \pm 0.0061$	$0.9882(0.9902) \pm 0.0065$	$0.9849(0.9874) \pm 0.0057$
$\tau_{\rm reio}$	$0.0590(0.0590)^{+0.0063}_{-0.0079}$	$0.0592(0.0573)^{+0.0069}_{-0.0080}$	$0.0573(0.0583)^{+0.0066}_{-0.0078}$
S_8	$0.836(0.836) \pm 0.011$	$0.831(0.842) \pm 0.012$	$0.836(0.841) \pm 0.012$
Ω_m	$0.2995(0.2997) \pm 0.0047$	$0.2985(0.3018) \pm 0.0049$	$0.3000(0.3001) \pm 0.0047$
$\Delta\chi^2_{\rm min}$	−35.1	−27.9	−24.1
ΔAIC	−29.1	−19.9	−20.1
$Q_{\rm DMAP}$	2.5σ	3.6σ	3.9σ

constraints from Pantheon+ may reduce the contribution of $f_{\rm ADE}$ and the value of H_0. These are in fact stable when compared to analyses with the older Pantheon data, with similar error bars between the EFT + Pan + M_b and EFT + PanPlus + M_b analyses. Thus, if we rely solely on the posterior distributions, we could argue that the Pantheon+ data do not change the conclusion about the ADE resolution of the Hubble tension. However, it turns out that the ADE model is not able to accommodate at the same time the large values of H_0 and Ω_m that are favored by the Pantheon+ data once they are calibrated with M_b. Indeed, the best-fit value $H_0 = 71.29$ km/s/Mpc is 1.7σ lower than the SH_0ES constraint [$H_0 = (73.04 \pm 1.04)$ km/s/Mpc], while the best-fit value $\Omega_m = 0.3014$ is 1.8σ lower than the Pantheon+ constraint ($\Omega_m = 0.334 \pm 0.018$). Therefore, the ADE model does not provide a good fit to the M_b prior ($\chi^2_{M_b} = 6.42$ as shown in Table III of Appendix B), while the fit to the Pantheon+ data is worse (by +1.6) with the inclusion of the M_b prior. These degradations of $\chi^2_{\rm min}$[9] imply that the $Q_{\rm DMAP}$ changes from 2.9σ (5.6σ for ΛCDM) to 3.6σ (6.3σ for ΛCDM) when we consider the Pantheon+ data (see Table I), which severely limits the ability of this model to resolve the H_0 tension. One of the two criteria of Ref. [15], namely, $Q_{\rm DMAP} < 3\sigma$, is indeed no longer fulfilled. However, while the Pantheon+ data and the M_b prior from Ref. [2] seriously restrict the ability of the ADE model to resolve the Hubble tension, these data improve the preference for this model over ΛCDM, since the ΔAIC changes from −18.9 to −21.8. We nevertheless caution overinterpreting this preference, given that the $Q_{\rm DMAP}$ indicates that combining these datasets is not statistically consistent. In addition, the Gaussian tension GT = 4.4σ is stable with respect to the EFT + Pan dataset.[10]

In the left panel of Fig. 4, we show the 2D posterior distributions of the axionlike EDE model reconstructed from the EFT + PanPlus + M_b dataset, while the associated cosmological constraints are displayed in Table II. For the axionlike EDE case, we find that the $Q_{\rm DMAP}$ changes from 2.4σ to 2.5σ, and that the ΔAIC changes from −22.9 to −29.1 between the old and the new Pantheon data analysis (see Table III of Appendix B for the individual $\chi^2_{\rm min}$). This model better supports these new data, since the $Q_{\rm DMAP}$ is stable (and especially the $\chi^2_{\rm min}$ of the SH_0ES prior), while the ΔAIC, as in the case of the ADE model, decreases significantly. Whereas with the addition of the EFT data we had a slight preference for EDE over ADE, with the Pantheon+ data the preference for this model becomes clearly apparent: In the axionlike EDE model, $H_0 = 71.67 \pm 0.77$ km/s/Mpc with $Q_{\rm DMAP} = 2.5\sigma$, while in the ADE model, $H_0 = 71.13 \pm 0.73$ km/s/Mpc with

[9]Let us note that the $\chi^2_{\rm min}$ of the other likelihoods are stable between the Pantheon and Pantheon+ analyses, and therefore play no role in the change in $Q_{\rm DMAP}$ between these two analyses.

[10]Note that for the same dataset, we obtain GT = 3.8σ for the axionlike EDE model and GT = 4.8σ for the ΛCDM model.

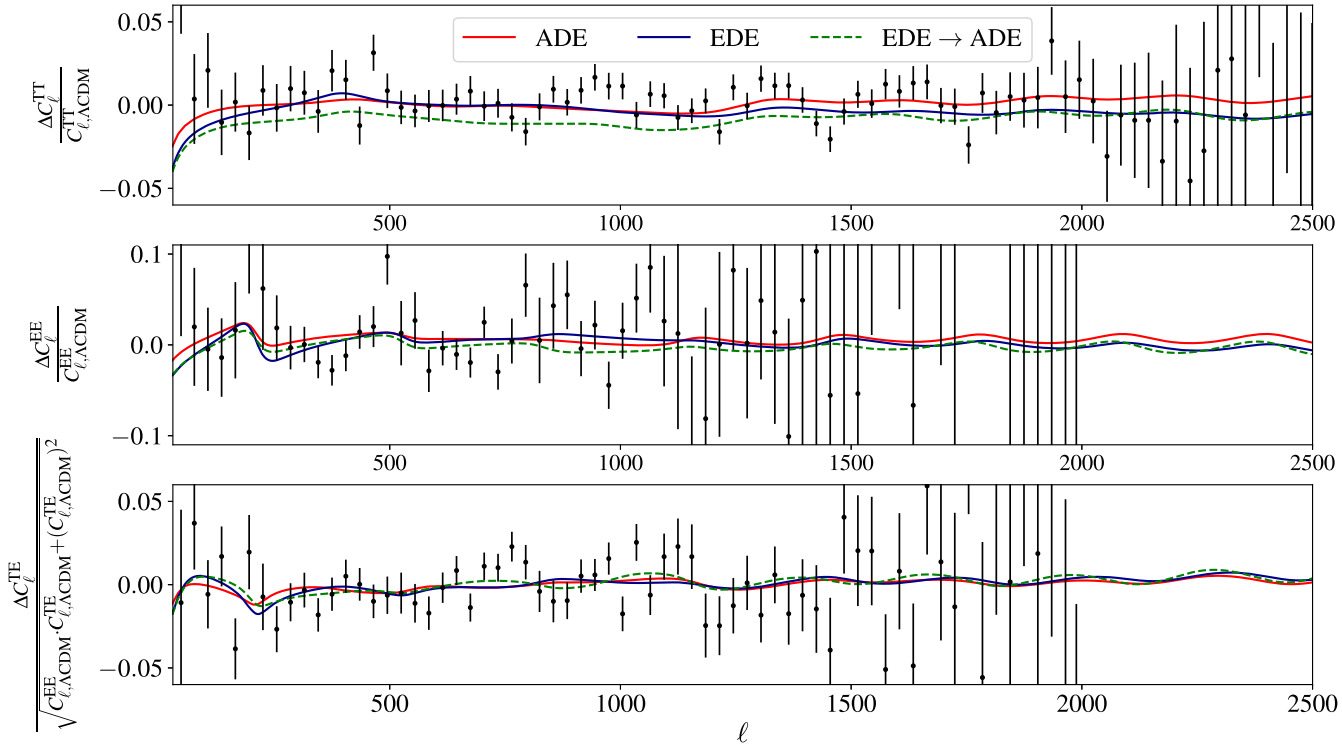

FIG. 3. CMB power spectra residuals with respect to ΛCDM for the ADE (red) and axionlike EDE (black) models. All cosmological parameters of the ΛCDM, ADE, and axionlike EDE models have been set to their EFT + PanPlus best fits, while the displayed data (normalized to the ΛCDM best fit) correspond to the *Planck* 2018 data [99]. Finally, for the plot titled "EDE → ADE," we set the ΛCDM parameters to the axionlike EDE best fit, while the z_c and w_f parameters are set to the ADE best fit. The last ADE parameter, namely, $f_{\rm ADE}(z_c) = 0.095$, is determined such that the values of $100\theta_s = 1.042$ and $r_s = 140.53$ Mpc are the same as for the EDE best fit.

$Q_{\rm DMAP} = 3.6\sigma$. In addition, the axionlike EDE model provides a better overall fit than the ADE model, with $\Delta AIC(\text{EDE} - \text{ADE}) = +7.3$. The two main contributions to this difference come from the *Planck* data (and in particular the high-ℓTTTEEE likelihood), where $\Delta\chi^2(\text{EDE} - \text{ADE}) = +3.7$, and from the S$H_0$ES prior, where $\Delta\chi^2(\text{EDE} - \text{ADE}) = +2.7$. The axionlike EDE model is capable of better compensating the effect of large values of H_0 and $\Omega_{\rm m}$ (and therefore $\omega_{\rm cdm}$) on the CMB compared to the ADE model.

In order to understand why the axionlike EDE model performs better than ADE, we plot in Fig. 3 the CMB power spectra residuals with respect to the ΛCDM best fit for these two models. In this figure, we also plot (in green dashed) the CMB power spectra residuals of the ADE model, where we set the ΛCDM parameters to the axionlike EDE best fit and the z_c and w_f parameters to the ADE best fit. The last ADE parameter, namely, $f_{\rm ADE}(z_c)$, is determined such that the values of the angular acoustic scale at recombination θ_* and the comoving sound horizon at recombination r_* are the same as for the EDE best fit. In other words, this plot would represent the best fit of the ADE model if the latter could reduce the Hubble tension to the same level as the axionlike EDE model. In this figure, the main difference between the ADE and ADE → EDE plots stems from the suppression (particularly at low ℓ) of the $C_\ell^{\rm TT}$ power spectrum for the EDE → ADE analysis. This suppression typically corresponds to the effect of a large value of $\omega_{\rm cdm}$ (and also n_s), showing that the ADE model is not able to compensate for a high value of $\Omega_{\rm cdm}h^2$ in the same way as the axionlike EDE model. This is explained by the fact that the EDE model allows the sound speed to decrease in the k range associated with $\ell < 500$, making it easier to compensate for the effect of increasing $\Omega_{\rm cdm}h^2$ in the low-ℓTT power spectrum. Let us note that the effect of the increase in $\Omega_{\rm cdm}h^2$ is more significant for the modes that have reentered the horizon at the time when $f_{\rm ADE}$ is decreasing, and therefore no longer significantly suppresses the evolution of the growing modes. In order to compensate for this effect, it is therefore helpful to decrease c_s^2 for $l < 500$, insofar as a reduction in this parameter leads to an enhancement in the Weyl potential (see Ref. [40]). Note that these results are compatible with Ref. [40], but interestingly the limitation in the value of $\Omega_{\rm cdm}h^2$ does not arise from the CMB polarization as in that reference (which considered *Planck* 2015 data), but from the CMB temperature.

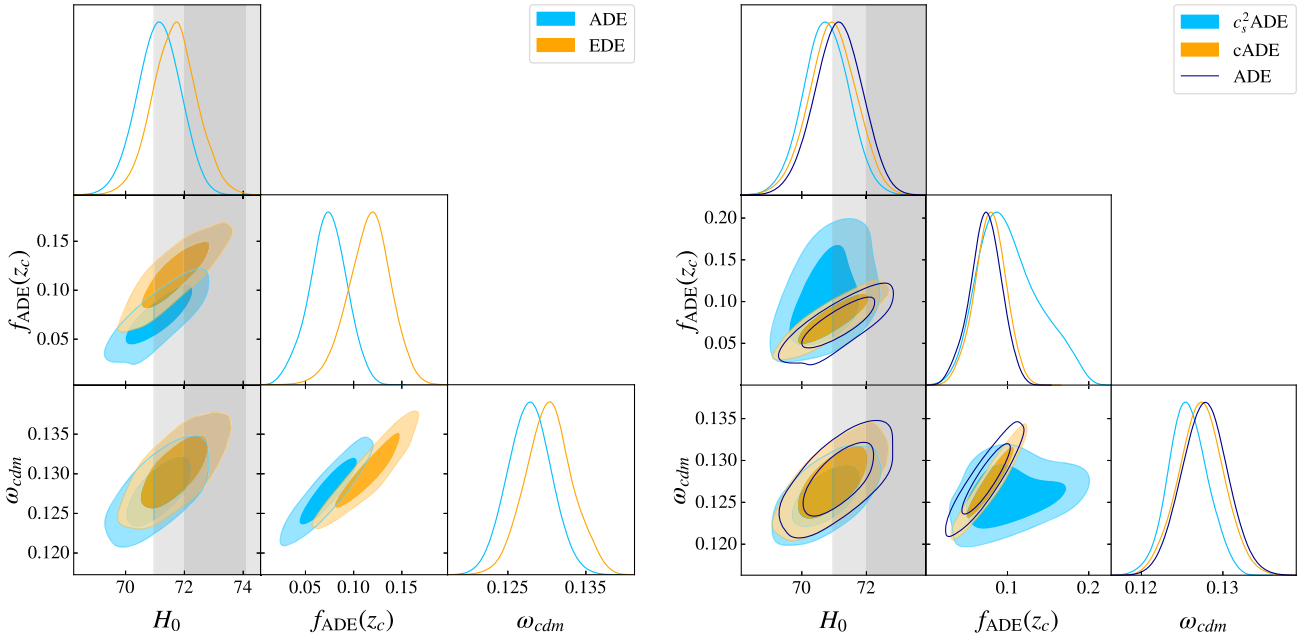

FIG. 4. Left panel: 2D posterior distributions reconstructed from the *Planck* + ext-BAO + EFT + PanPlus + M_b dataset, i.e., the most up-to-date dataset, for our baseline ADE model and the standard axionlike EDE model. Right panel: 2D posterior distributions reconstructed from the *Planck* + ext-BAO + EFT + PanPlus + M_b dataset for the c_s^2ADE model (namely, our baseline ADE model with the variation of c_s^2), the cADE model (namely, our baseline ADE model with $c_s^2 = w_f = 1$), and our baseline ADE model. The gray bands correspond to the H_0 constraint associated with the M_b prior $H_0 = (73.04 \pm 1.04)$ km/s/Mpc [2].

IV. MODEL VARIATIONS

A. Variation of c_s^2

In the previous sections, we fixed $c_s^2(a_c) = w_f$ instead of varying these two parameters independently. In the right panel of Fig. 4, we show the 2D posterior distributions reconstructed from the EFT + PanPlus + M_b dataset for our baseline ADE model by relaxing this assumption, while in Table II we display the associated cosmological constraints. To do so, we have applied the prior of Refs. [40,41] to c_s^2, namely,

$$0 \leq c_s^2 \leq 1.5.$$

In the following, we simply call this extended model "c_s^2ADE," for which we still consider that $p = 1$. Interestingly, and in line with Ref. [40], the assumption $c_s^2 = w_f$ does not change our conclusions, especially regarding the Hubble tension: We obtain $Q_{\rm DMAP} = 3.6\sigma$, which is similar to that of our baseline ADE model (see Table III of Appendix B for the χ^2 values). In this specific case, we obtain $H_0 = 70.76 \pm 0.70$ km/s/Mpc, which is 0.5σ lower than the H_0 value from our baseline ADE model. This is due to projection effects caused by the non-Gaussian posteriors of c_s^2 and w_f, and we notice that the best-fit value ($H_0 = 71.23$ km/s/Mpc) is very close to that of the ADE model. Thus, the relaxation of this hypothesis does not resolve the Hubble tension, while the ΔAIC worsens somewhat in this model because of the additional parameter ($\Delta AIC = -20.1$ instead of -21.8 for our baseline ADE model). In addition, as shown in Fig. 5, the best-fit point of the ADE model in the $c_s^2 - w_f$ plane lies in the 68% C.L. reconstructed from the c_s^2ADE model and is very close to the best-fit point of this model. This implies that setting $c_s^2 = w_f$ is a good approximation around the best fit of the c_s^2ADE model.

B. The cADE model

References [40,41] showed that the special case where $c_s^2 = w_f = 1$ made it possible to solve the Hubble tension. In this particular model called "cADE," the ADE component is a canonical scalar which goes from a frozen phase ($w = -1$) to a kinetion phase ($w = 1$) around matter-radiation equality. This model is particularly interesting because it allows the Hubble tension to be resolved with only two more parameters than the ΛCDM model [namely, $f_{\rm ADE}(z_c)$ and $\log_{10}(z_c)$]. However, while in Ref. [40] the case $c_s^2 = w_f = 1$ is within the 68% C.L. of the c_s^2 and w_f parameters (see Fig. 1 of this reference), one can see in Fig. 5 that this particular case is no longer located in the 1σ region.[11] In the right panel of Fig. 4, we display the 2D posterior distributions of the cADE model reconstructed

[11]Let us note that Refs. [40,41] set $p = 1/2$, while we set $p = 1$, but this difference does not change the results.

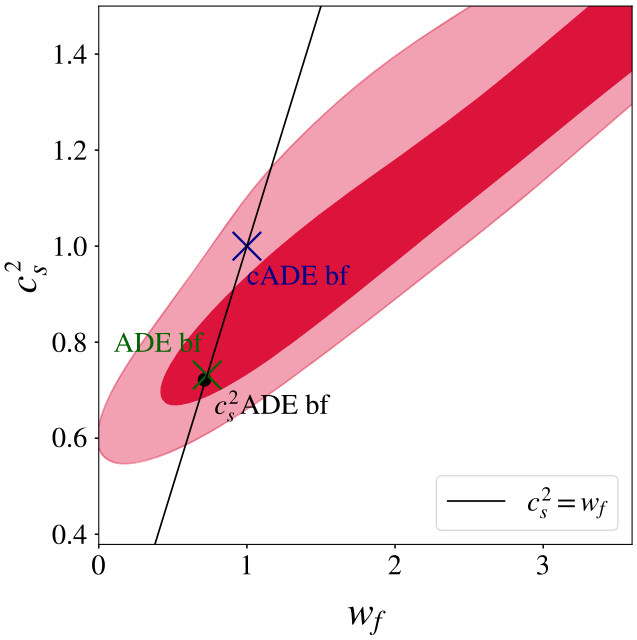

FIG. 5. 2D posterior distribution of the $c_s^2 - w_f$ plane reconstructed from the *Planck* + ext-BAO + EFT + PanPlus + M_b dataset for the c_s^2ADE model. The solid line corresponds to $c_s^2 = w_f$, while the blue and green crosses correspond, respectively, to the cADE model and the best fit of our baseline ADE model. The black circle represents the best fit of the c_s^2ADE model.

from the EFT + PanPlus + M_b dataset, while in Table II we display the associated cosmological constraints. We can clearly see that this particular model is unable to resolve the Hubble tension with current data, since we obtain $H_0 = 70.95 \pm 0.73$ km/s/Mpc and $f_{\rm ADE}(z_c) = 0.079 \pm 0.019$, with a $Q_{\rm DMAP} = 3.9\sigma$ (compared to $Q_{\rm DMAP} = 3.6\sigma$ for our baseline ADE model).

V. CONCLUSION

In this paper, we have updated the constraints on the acoustic dark energy and axionlike early dark energy models by first assessing the impact of the EFT full-shape analysis applied to the BOSS LRG and eBOSS QSO data, and second, the impact of the latest Pantheon+ data.

(i) When we consider the full-shape analysis of the BOSS and eBOSS data combined with *Planck*, ext-BAO measurements, Pantheon data from [111], and SH_0ES data from [2], we obtain $H_0 = 71.01 \pm 0.73$ km/s/Mpc with a residual Hubble tension of 2.9σ (compared to 2.4σ for the axionlike EDE model and 5.6σ for the ΛCDM model).

(ii) We have demonstrated that the EFTofLSS analysis slightly reduces the ability of this model to resolve the Hubble tension compared to the BAO/$f\sigma_8$ analysis, which has a residual tension of 2.6σ (with $H_0 = 71.24 \pm 0.68$ km/s/Mpc).

(iii) Although the axionlike EDE model remains a better solution to the Hubble tension after using the EFTofBOSS and EFTofeBOSS likelihoods, we have shown that the EFTofLSS analysis has a stronger impact on this model.

(iv) Importantly, when we replace the Pantheon data with the Pantheons+ data from [44], the ADE model no longer resolves the Hubble tension at a suitable level, leading to a 3.6σ residual tension (compared to 2.5σ for the EDE model and 6.3σ for the ΛCDM model).

(v) Whereas with the EFTofLSS analysis we had only a slight preference for EDE over ADE, with the new data from Pantheon+ and SH_0ES, the preference for this model became clearly apparent, due to the fact that axionlike EDE manages to compensate a higher $\Omega_{\rm cdm}h^2$ in *Planck* data thanks to the scale dependence of the sound speed.

(vi) Finally, we have verified that relaxing the assumption $c_s^2 = w_f$ does not alter our conclusions, justifying this choice. In addition, for the cADE model (where $c_s^2 = w_f = 1$), we have obtained $H_0 = 70.95 \pm 0.73$ km/s/Mpc with a $Q_{\rm DMAP} = 3.9\sigma$, implying that one can no longer solve the Hubble tension with this constrained ADE model, contrary to previous results [40,41].

Let us add a few words about the $S_8 \equiv \sigma_8 \cdot \sqrt{\Omega_m/0.3}$ tension (see, e.g., Ref. [116] for a review). EDE-like models are known to slightly increase the amplitude of fluctuations σ_8 with respect to ΛCDM [17,31,117] due to an increase in $\omega_{\rm cdm}$ and n_s. In particular, increasing $\omega_{\rm cdm}$ brings forward matter-radiation equality $a_{\rm eq}$, leaving more time for growing modes (that are subhorizon at $a_{\rm eq}$) to evolve in the matter era. Considering our most up-to-date dataset (i.e., EFT + PanPlus + M_b), we have obtained a Gaussian tension[12] on S_8 of 3.2σ, 3.5σ, and 3.8σ for the ΛCDM, ADE, and axionlike EDE models, respectively. It is interesting to note that the better the model is able to resolve the Hubble tension, the higher the S_8 tension. In order to resolve these two tensions simultaneously in the context of EDE cosmologies, it is therefore necessary to find a mechanism that reduces the growth of small-scale modes, as could be achieved by an interaction between EDE and DM [120].

[12]We use here the Gaussian metric $(\theta_i - \theta_j)/\sqrt{\sigma_{\theta,i}^2 + \sigma_{\theta,j}^2}$, where θ_i and $\sigma_{\theta,i}$ are, respectively, the mean value and the standard deviation of the parameter θ for the dataset i. For the week lensing determination of the S_8 parameter, we use the simple weighted mean and uncertainty of $S_8^{\rm GT} = 0.766^{+0.020}_{-0.014}$ from the combination of KiDS-1000 × dFLensS + BOSS $S_8 = 0.769^{+0.016}_{-0.012}$ [118] and DES-Y3 $S_8 = 0.775^{+0.026}_{-0.024}$ [119].

In this paper, we have shown that the new data from Pantheon and SH_0ES, and to a lesser extent the EFTofLSS applied to the BOSS and eBOSS data, can have a decisive impact on models which aim to resolve the Hubble tension. We leave for future work the study of the impact on the Hubble tension of such an analysis applied to other early dark energy models, such as new early dark energy [19,20], rock "n" roll dark energy [22], or early modified gravity [25,121].

ACKNOWLEDGMENTS

The author would like to warmly thank Vivian Poulin and Tristan L. Smith for their comments and insights throughout the project. Much of this work was carried out during a four-week visit to the Center for Theoretical Physics (CTP) at the Massachusetts Institute of Technology. The author would therefore like to express his gratitude to the members of the CTP, and in particular to Tracy Slatyer, for their hospitality and kindness. These results have been made possible thanks to LUPM's cloud computing infrastructure founded by Ocevu labex, and France-Grilles. This project has received support from the European Union's Horizon 2020 research and innovation program under the Marie Sklodowska-Curie Grant Agreement No. 860881-HIDDeN. This project has also received funding from the European Research Council under the European Union's HORIZON-ERC-2022 (Grant Agreement No. 101076865).

APPENDIX A: M_b PRIOR

In this appendix, we show explicitly, thanks to Fig. 6, that the addition of the M_b prior [2] on top of the Pantheon+ likelihood is equivalent to the use of the full Pantheon + /SH_0ES likelihood as provided in Ref. [2]. Since the constraints are similar, we have chosen to show in this paper the results with the M_b prior, for the sake of convenience, in order to determine the $Q_{\rm DMAP}$ values easily.

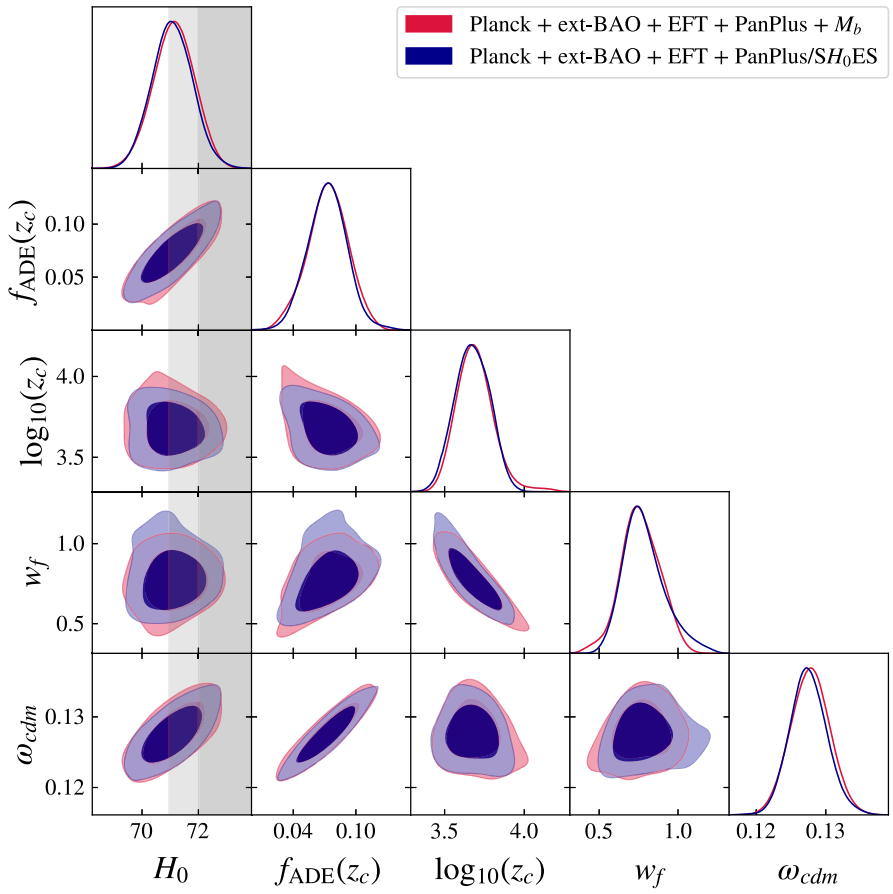

FIG. 6. 2D posterior distributions reconstructed from *Planck* + ext-BAO + EFT, either with the M_b prior on top of the Pantheon+ likelihood, or with the cross-correlation between the Pantheon+ data and the SH_0ES data (namely, the Pantheon + /SH_0ES likelihood) as provided in Ref. [2]. The gray band corresponds to the H_0 constraint associated with the M_b prior $H_0 = (73.04 \pm 1.04)$ km/s/Mpc [2].

TABLE III. Table of best-fit χ^2 of the different models considered in this work for various combinations of likelihood. All datasets include *Planck* + ext-BAO data. Note that the columns "BOSS" and "eBOSS" refer either to the BAO/$f\sigma_8$ analysis or to the EFT full-shape analysis. Similarly, the column "Pan" refers to either Pantheon data or Pantheon+ data. Finally, "PanPlus/SH_0ES" corresponds to the full Pantheon + /SH_0ES likelihood as provided in Ref. [2].

Data	Model	χ^2 tot	P18TTTEE	P18lens	ext-BAO	BOSS	eBOSS	Pan	M_b	PanPlus/SH_0ES
BAO/$f\sigma_8$ + Pan	ΛCDM	3816.39	2763.03	8.87	1.38	6.15	9.88	1027.07	···	···
	ADE	3812.50	2759.48	9.14	1.30	6.55	8.92	1027.10	···	···
	EDE	3809.87	2757.41	9.70	1.64	6.30	7.89	1026.93	···	···
BAO/$f\sigma_8$ + Pan + M_b	ΛCDM	3847.33	2765.48	9.12	1.84	5.91	9.14	1026.89	28.94	···
	ADE	3819.06	2763.73	10.09	1.77	6.95	6.32	1026.89	3.32	···
	EDE	3812.26	2759.10	9.89	1.91	6.97	6.21	1026.87	1.31	···
EFT + Pan	ΛCDM	4020.07	2762.14	8.87	1.25	160.20	60.44	1027.17	···	···
	ADE	4018.67	2761.21	8.99	1.40	159.63	60.39	1027.06	···	···
	EDE	4017.09	2759.20	9.29	1.60	159.54	60.51	1026.95	···	···
EFT + Pan + M_b	ΛCDM	4051.76	2764.81	9.13	1.78	158.30	61.16	1026.90	29.61	···
	ADE	4026.87	2763.76	9.62	2.11	159.94	60.26	1026.86	4.33	···
	EDE	4022.83	2758.51	9.60	1.99	160.36	61.64	1026.87	3.86	···
EFT + PanPlus	ΛCDM	4404.28	2762.12	8.78	1.20	160.44	60.43	1411.31	···	···
	cADE	4404.07	2761.57	8.86	1.20	160.68	60.46	1411.31	···	···
	ADE	4402.96	2760.49	8.89	1.21	160.78	60.23	1411.36	···	···
	c_s^2ADE	4402.93	2760.47	8.90	1.21	160.76	60.23	1411.37	···	···
	EDE	4402.54	2758.74	9.02	1.38	160.38	61.21	1411.82	···	···
EFT + PanPlus + M_b	ΛCDM	4443.78	2766.95	9.69	1.95	158.36	60.63	1413.17	33.02	···
	cADE	4419.67	2766.20	9.67	1.92	160.68	61.17	1413.27	6.76	···
	ADE	4415.94	2763.42	9.82	1.81	160.52	60.95	1412.99	6.42	···
	c_s^2ADE	4415.89	2763.16	9.82	1.77	160.58	60.96	1412.91	6.70	···
	EDE	4408.67	2759.71	10.05	1.96	159.64	60.24	1413.35	3.72	···
EFT + PanPlus/SH_0ES	ΛCDM	4318.12	2767.42	9.24	2.20	158.01	60.39	···	···	1320.85
	ADE	4292.12	2763.74	9.77	1.94	160.31	60.20	···	···	1296.17

APPENDIX B: χ^2 TABLE

In this appendix, we report the best-fit χ^2 per experiment for the ΛCDM model, the ADE model, as well as the axionlike EDE model for several combinations of data.

[1] N. Aghanim *et al.* (Planck Collaboration), Planck 2018 results. VI. Cosmological parameters, Astron. Astrophys. **641**, A6 (2020); **652**, C4(E) (2021).

[2] Adam G. Riess *et al.*, A comprehensive measurement of the local value of the Hubble constant with 1 km/s/Mpc uncertainty from the Hubble space telescope and the SH0ES Team, Astrophys. J. Lett. **934**, L7 (2022).

[3] Adam G. Riess, Louise Breuval, Wenlong Yuan, Stefano Casertano, Lucas M. Macri, J. Bradley Bowers, Dan Scolnic, Tristan Cantat-Gaudin, Richard I. Anderson, and Mauricio Cruz Reyes, Cluster Cepheids with high precision Gaia parallaxes, low zero-point uncertainties, and Hubble space telescope photometry, Astrophys. J. **938**, 36 (2022).

[4] Maria Giovanna Dainotti, Biagio De Simone, Tiziano Schiavone, Giovanni Montani, Enrico Rinaldi, and Gaetano Lambiase, On the Hubble constant tension in the SNe Ia Pantheon sample, Astrophys. J. **912**, 150 (2021).

[5] Maria Giovanna Dainotti, Biagio De Simone, Tiziano Schiavone, Giovanni Montani, Enrico Rinaldi, Gaetano Lambiase, Malgorzata Bogdan, and Sahil Ugale, On the evolution of the Hubble constant with the SNe Ia Pantheon sample and baryon acoustic oscillations: A feasibility

study for GRB-cosmology in 2030, Galaxies **10**, 24 (2022).
[6] Edvard Mortsell, Ariel Goobar, Joel Johansson, and Suhail Dhawan, Sensitivity of the Hubble constant determination to Cepheid calibration, Astrophys. J. **933**, 212 (2022).
[7] Edvard Mortsell, Ariel Goobar, Joel Johansson, and Suhail Dhawan, The Hubble tension revisited: Additional local distance ladder uncertainties, Astrophys. J. **935**, 58 (2022).
[8] Brent Follin and Lloyd Knox, Insensitivity of the distance ladder Hubble constant determination to Cepheid calibration modelling choices, Mon. Not. R. Astron. Soc. **477**, 4534 (2018).
[9] Dillon Brout and Daniel Scolnic, It's dust: Solving the mysteries of the intrinsic scatter and host-galaxy dependence of standardized type Ia supernova brightnesses, Astrophys. J. **909**, 26 (2021).
[10] Jose Luis Bernal, Licia Verde, and Adam G. Riess, The trouble with H_0, J. Cosmol. Astropart. Phys. 10 (2016) 019.
[11] Kevin Aylor, MacKenzie Joy, Lloyd Knox, Marius Millea, Srinivasan Raghunathan, and W. L. Kimmy Wu, Sounds discordant: Classical distance ladder & ΛCDM-based determinations of the cosmological sound horizon, Astrophys. J. **874**, 4 (2019).
[12] Lloyd Knox and Marius Millea, Hubble constant hunter's guide, Phys. Rev. D **101**, 043533 (2020).
[13] David Camarena and Valerio Marra, On the use of the local prior on the absolute magnitude of type Ia supernovae in cosmological inference, Mon. Not. R. Astron. Soc. **504**, 5164 (2021).
[14] George Efstathiou, To H_0 or not to H_0?, Mon. Not. R. Astron. Soc. **505**, 3866 (2021).
[15] Nils Schöneberg, Guillermo Franco Abellán, Andrea Pérez Sánchez, Samuel J. Witte, Vivian Poulin, and Julien Lesgourgues, The H_0 Olympics: A fair ranking of proposed models, Phys. Rep. **984**, 1 (2022).
[16] Tanvi Karwal and Marc Kamionkowski, Dark energy at early times, the Hubble parameter, and the string axiverse, Phys. Rev. D **94**, 103523 (2016).
[17] Vivian Poulin, Tristan L. Smith, Tanvi Karwal, and Marc Kamionkowski, Early dark energy can resolve the Hubble tension, Phys. Rev. Lett. **122**, 221301 (2019).
[18] Tristan L. Smith, Vivian Poulin, and Mustafa A. Amin, Oscillating scalar fields and the Hubble tension: A resolution with novel signatures, Phys. Rev. D **101**, 063523 (2020).
[19] Florian Niedermann and Martin S. Sloth, New early dark energy, Phys. Rev. D **103**, L041303 (2021).
[20] Florian Niedermann and Martin S. Sloth, Resolving the Hubble tension with new early dark energy, Phys. Rev. D **102**, 063527 (2020).
[21] Gen Ye and Yun-Song Piao, Is the Hubble tension a hint of AdS phase around recombination?, Phys. Rev. D **101**, 083507 (2020).
[22] Prateek Agrawal, Francis-Yan Cyr-Racine, David Pinner, and Lisa Randall, Rock "n" roll solutions to the Hubble tension, Phys. Dark Universe **42**, 101347 (2023).
[23] Kim V. Berghaus and Tanvi Karwal, Thermal friction as a solution to the Hubble tension, Phys. Rev. D **101**, 083537 (2020).
[24] Matteo Braglia, William T. Emond, Fabio Finelli, A. Emir Gumrukcuoglu, and Kazuya Koyama, Unified framework for early dark energy from α-attractors, Phys. Rev. D **102**, 083513 (2020).
[25] Matteo Braglia, Mario Ballardini, Fabio Finelli, and Kazuya Koyama, Early modified gravity in light of the H_0 tension and LSS data, Phys. Rev. D **103**, 043528 (2021).
[26] Mark Gonzalez, Mark P. Hertzberg, and Fabrizio Rompineve, Ultralight scalar decay and the Hubble tension, J. Cosmol. Astropart. Phys. 10 (2020) 028.
[27] K. Rezazadeh, A. Ashoorioon, and D. Grin, Cascading dark energy, arXiv:2208.07631.
[28] Laura Herold, Elisa G. M. Ferreira, and Eiichiro Komatsu, New constraint on early dark energy from Planck and BOSS data using the profile likelihood, Astrophys. J. Lett. **929**, L16 (2022).
[29] Adrià Gómez-Valent, Fast test to assess the impact of marginalization in Monte Carlo analyses and its application to cosmology, Phys. Rev. D **106**, 063506 (2022).
[30] Vivian Poulin, Tristan L. Smith, and Alexa Bartlett, Dark energy at early times and ACT: A larger Hubble constant without late-time priors, Phys. Rev. D **104**, 123550 (2021).
[31] J. Colin Hill, Evan McDonough, Michael W. Toomey, and Stephon Alexander, Early dark energy does not restore cosmological concordance, Phys. Rev. D **102**, 043507 (2020).
[32] Adrien La Posta, Thibaut Louis, Xavier Garrido, and J. Colin Hill, Constraints on pre-recombination early dark energy from SPT-3G public data, Phys. Rev. D **105**, 083519 (2022).
[33] Alexander Reeves, Laura Herold, Sunny Vagnozzi, Blake D. Sherwin, and Elisa G. M. Ferreira, Restoring cosmological concordance with early dark energy and massive neutrinos?, Mon. Not. R. Astron. Soc. **520**, 3688 (2023).
[34] Laura Herold and Elisa G. M. Ferreira, Resolving the Hubble tension with early dark energy, Phys. Rev. D **108**, 043513 (2023).
[35] Johannes R. Eskilt, Laura Herold, Eiichiro Komatsu, Kai Murai, Toshiya Namikawa, and Fumihiro Naokawa, Constraints on early dark energy from isotropic cosmic birefringence, Phys. Rev. Lett. **131**, 121001 (2023).
[36] Riccardo Murgia, Guillermo F. Abellán, and Vivian Poulin, Early dark energy resolution to the Hubble tension in light of weak lensing surveys and lensing anomalies, Phys. Rev. D **103**, 063502 (2021).
[37] Samuel Goldstein, J. Colin Hill, Vid Iršič, and Blake D. Sherwin, Canonical Hubble-tension-resolving early dark energy cosmologies are inconsistent with the Lyman-α forest, Phys. Rev. Lett. **131**, 201001 (2023).
[38] Vivian Poulin, Tristan L. Smith, and Tanvi Karwal, The ups and downs of early dark energy solutions to the Hubble tension: A review of models, hints and constraints circa 2023, Phys. Dark Universe **42**, 101348 (2023).
[39] Eleonora Di Valentino, Olga Mena, Supriya Pan, Luca Visinelli, Weiqiang Yang, Alessandro Melchiorri, David F. Mota, Adam G. Riess, and Joseph Silk, In the realm of the Hubble tension—A review of solutions, Classical Quantum Gravity **38**, 153001 (2021).

[40] Meng-Xiang Lin, Giampaolo Benevento, Wayne Hu, and Marco Raveri, Acoustic dark energy: Potential conversion of the Hubble tension, Phys. Rev. D **100**, 063542 (2019).
[41] Meng-Xiang Lin, Wayne Hu, and Marco Raveri, Testing H_0 in acoustic dark energy with Planck and ACT polarization, Phys. Rev. D **102**, 123523 (2020).
[42] Shadab Alam *et al.* (BOSS Collaboration), The clustering of galaxies in the completed SDSS-III Baryon Oscillation Spectroscopic Survey: Cosmological analysis of the DR12 galaxy sample, Mon. Not. R. Astron. Soc. **470**, 2617 (2017).
[43] Shadab Alam *et al.* (eBOSS Collaboration), Completed SDSS-IV extended Baryon Oscillation Spectroscopic Survey: Cosmological implications from two decades of spectroscopic surveys at the Apache Point Observatory, Phys. Rev. D **103**, 083533 (2021).
[44] Dillon Brout *et al.*, The Pantheon+ analysis: Cosmological constraints, Astrophys. J. **938**, 110 (2022).
[45] John Joseph M. Carrasco, Mark P. Hertzberg, and Leonardo Senatore, The effective field theory of cosmological large scale structures, J. High Energy Phys. 09 (2012) 082.
[46] Daniel Baumann, Alberto Nicolis, Leonardo Senatore, and Matias Zaldarriaga, Cosmological non-linearities as an effective fluid, J. Cosmol. Astropart. Phys. 07 (2012) 051.
[47] Rafael A. Porto, Leonardo Senatore, and Matias Zaldarriaga, The Lagrangian-space effective field theory of large scale structures, J. Cosmol. Astropart. Phys. 05 (2014) 022.
[48] Enrico Pajer and Matias Zaldarriaga, On the renormalization of the effective field theory of large scale structures, J. Cosmol. Astropart. Phys. 08 (2013) 037.
[49] Ali Akbar Abolhasani, Mehrdad Mirbabayi, and Enrico Pajer, Systematic renormalization of the effective theory of large scale structure, J. Cosmol. Astropart. Phys. 05 (2016) 063.
[50] Leonardo Senatore and Matias Zaldarriaga, Redshift space distortions in the effective field theory of large scale structures, arXiv:1409.1225.
[51] Tobias Baldauf, Mehrdad Mirbabayi, Marko Simonović, and Matias Zaldarriaga, Equivalence principle and the baryon acoustic peak, Phys. Rev. D **92**, 043514 (2015).
[52] Leonardo Senatore and Matias Zaldarriaga, The IR-resummed effective field theory of large scale structures, J. Cosmol. Astropart. Phys. 02 (2015) 013.
[53] Leonardo Senatore and Gabriele Trevisan, On the IR-resummation in the EFTofLSS, J. Cosmol. Astropart. Phys. 05 (2018) 019.
[54] Matthew Lewandowski and Leonardo Senatore, An analytic implementation of the IR-resummation for the BAO peak, J. Cosmol. Astropart. Phys. 03 (2020) 018.
[55] Diego Blas, Mathias Garny, Mikhail M. Ivanov, and Sergey Sibiryakov, Time-sliced perturbation theory II: Baryon acoustic oscillations and infrared resummation, J. Cosmol. Astropart. Phys. 07 (2016) 028.
[56] John Joseph M. Carrasco, Simon Foreman, Daniel Green, and Leonardo Senatore, The 2-loop matter power spectrum and the IR-safe integrand, J. Cosmol. Astropart. Phys. 07 (2014) 056.
[57] John Joseph M. Carrasco, Simon Foreman, Daniel Green, and Leonardo Senatore, The effective field theory of large scale structures at two loops, J. Cosmol. Astropart. Phys. 07 (2014) 057.
[58] Leonardo Senatore, Bias in the effective field theory of large scale structures, J. Cosmol. Astropart. Phys. 11 (2015) 007.
[59] Mehrdad Mirbabayi, Fabian Schmidt, and Matias Zaldarriaga, Biased tracers and time evolution, J. Cosmol. Astropart. Phys. 07 (2015) 030.
[60] Raul Angulo, Matteo Fasiello, Leonardo Senatore, and Zvonimir Vlah, On the statistics of biased tracers in the effective field theory of large scale structures, J. Cosmol. Astropart. Phys. 09 (2015) 029.
[61] Tomohiro Fujita, Valentin Mauerhofer, Leonardo Senatore, Zvonimir Vlah, and Raul Angulo, Very massive tracers and higher derivative biases, J. Cosmol. Astropart. Phys. 01 (2020) 009.
[62] Ashley Perko, Leonardo Senatore, Elise Jennings, and Risa H. Wechsler, Biased tracers in redshift space in the EFT of large-scale structure, arXiv:1610.09321.
[63] Ethan O. Nadler, Ashley Perko, and Leonardo Senatore, On the bispectra of very massive tracers in the effective field theory of large-scale structure, J. Cosmol. Astropart. Phys. 02 (2018) 058.
[64] Guido D'Amico, Jérôme Gleyzes, Nickolas Kokron, Katarina Markovic, Leonardo Senatore, Pierre Zhang, Florian Beutler, and Héctor Gil-Marín, The cosmological analysis of the SDSS/BOSS data from the effective field theory of large-scale structure, J. Cosmol. Astropart. Phys. 05 (2020) 005.
[65] Théo Simon, Pierre Zhang, and Vivian Poulin, Cosmological inference from the EFTofLSS: The eBOSS QSO full-shape analysis, J. Cosmol. Astropart. Phys. 07 (2023) 041.
[66] Mikhail M. Ivanov, Marko Simonović, and Matias Zaldarriaga, Cosmological parameters from the BOSS galaxy power spectrum, J. Cosmol. Astropart. Phys. 05 (2020) 042.
[67] Thomas Colas, Guido D'amico, Leonardo Senatore, Pierre Zhang, and Florian Beutler, Efficient cosmological analysis of the SDSS/BOSS data from the effective field theory of large-scale structure, J. Cosmol. Astropart. Phys. 06 (2020) 001.
[68] Guido D'Amico, Leonardo Senatore, and Pierre Zhang, Limits on wCDM from the EFTofLSS with the PyBird code, J. Cosmol. Astropart. Phys. 01 (2021) 006.
[69] Guido D'Amico, Yaniv Donath, Leonardo Senatore, and Pierre Zhang, Limits on clustering and smooth quintessence from the EFTofLSS, J. Cosmol. Astropart. Phys. 03 (2024) 032.
[70] Théo Simon, Guillermo Franco Abellán, Peizhi Du, Vivian Poulin, and Yuhsin Tsai, Constraining decaying dark matter with BOSS data and the effective field theory of large-scale structures, Phys. Rev. D **106**, 023516 (2022).
[71] Théo Simon, Pierre Zhang, Vivian Poulin, and Tristan L. Smith, Consistency of effective field theory analyses of the BOSS power spectrum, Phys. Rev. D **107**, 123530 (2023).
[72] Shi-Fan Chen, Zvonimir Vlah, and Martin White, A new analysis of galaxy 2-point functions in the BOSS survey,

including full-shape information and post-reconstruction BAO, J. Cosmol. Astropart. Phys. 02 (2022) 008.
[73] Pierre Zhang, Guido D'Amico, Leonardo Senatore, Cheng Zhao, and Yifu Cai, BOSS correlation function analysis from the effective field theory of large-scale structure, J. Cosmol. Astropart. Phys. 02 (2022) 036.
[74] Oliver H. E. Philcox and Mikhail M. Ivanov, BOSS DR12 full-shape cosmology: ΛCDM constraints from the large-scale galaxy power spectrum and bispectrum monopole, Phys. Rev. D **105**, 043517 (2022).
[75] Suresh Kumar, Rafael C. Nunes, and Priya Yadav, Updating non-standard neutrinos properties with Planck-CMB data and full-shape analysis of BOSS and eBOSS galaxies, J. Cosmol. Astropart. Phys. 09 (2022) 060.
[76] Rafael C. Nunes, Sunny Vagnozzi, Suresh Kumar, Eleonora Di Valentino, and Olga Mena, New tests of dark sector interactions from the full-shape galaxy power spectrum, Phys. Rev. D **105**, 123506 (2022).
[77] Alex Laguë, J. Richard Bond, Renée Hložek, Keir K. Rogers, David J. E. Marsh, and Daniel Grin, Constraining ultralight axions with galaxy surveys, J. Cosmol. Astropart. Phys. 01 (2022) 049.
[78] Oliver H. E. Philcox, Blake D. Sherwin, Gerrit S. Farren, and Eric J. Baxter, Determining the Hubble constant without the sound horizon: Measurements from galaxy surveys, Phys. Rev. D **103**, 023538 (2021).
[79] Tristan L. Smith, Vivian Poulin, and Théo Simon, Assessing the robustness of sound horizon-free determinations of the Hubble constant, Phys. Rev. D **108**, 103525 (2023).
[80] Chiara Moretti, Maria Tsedrik, Pedro Carrilho, and Alkistis Pourtsidou, Modified gravity and massive neutrinos: Constraints from the full shape analysis of BOSS galaxies and forecasts for Stage IV surveys, J. Cosmol. Astropart. Phys. 12 (2023) 025.
[81] Henrique Rubira, Asmaa Mazoun, and Mathias Garny, Full-shape BOSS constraints on dark matter interacting with dark radiation and lifting the S8 tension, J. Cosmol. Astropart. Phys. 01 (2023) 034.
[82] Nils Schöneberg, Guillermo Franco Abellán, Théo Simon, Alexa Bartlett, Yashvi Patel, and Tristan L. Smith, The weak, the strong and the ugly—A comparative analysis of interacting stepped dark radiation, Phys. Rev. D **108**, 123513 (2023).
[83] Emil Brinch Holm, Laura Herold, Théo Simon, Elisa G. M. Ferreira, Steen Hannestad, Vivian Poulin, and Thomas Tram, Bayesian and frequentist investigation of prior effects in EFTofLSS analyses of full-shape BOSS and eBOSS data, Phys. Rev. D **108**, 123514 (2023).
[84] Théo Simon, Pierre Zhang, Vivian Poulin, and Tristan L. Smith, Updated constraints from the effective field theory analysis of the BOSS power spectrum on early dark energy, Phys. Rev. D **107**, 063505 (2023).
[85] Guido D'Amico, Leonardo Senatore, Pierre Zhang, and Henry Zheng, The Hubble tension in light of the full-shape analysis of large-scale structure data, J. Cosmol. Astropart. Phys. 05 (2021) 072.
[86] Tristan L. Smith, Vivian Poulin, José Luis Bernal, Kimberly K. Boddy, Marc Kamionkowski, and Riccardo Murgia, Early dark energy is not excluded by current large-scale structure data, Phys. Rev. D **103**, 123542 (2021).
[87] Mikhail M. Ivanov, Evan McDonough, J. Colin Hill, Marko Simonović, Michael W. Toomey, Stephon Alexander, and Matias Zaldarriaga, Constraining early dark energy with large-scale structure, Phys. Rev. D **102**, 103502 (2020).
[88] Alain Blanchard, Jean-Yves Héloret, Stéphane Ilić, Brahim Lamine, and Isaac Tutusaus, ΛCDM is alive and well, Open J. Astrophys. **7**, 117170 (2024).
[89] Vivian Poulin, Tristan L. Smith, Daniel Grin, Tanvi Karwal, and Marc Kamionkowski, Cosmological implications of ultralight axionlike fields, Phys. Rev. D **98**, 083525 (2018).
[90] C. Armendariz-Picon, Viatcheslav F. Mukhanov, and Paul J. Steinhardt, Essentials of *k*-essence, Phys. Rev. D **63**, 103510 (2001).
[91] Christopher Gordon and Wayne Hu, A low CMB quadrupole from dark energy isocurvature perturbations, Phys. Rev. D **70**, 083003 (2004).
[92] Adrià Gómez-Valent, Ziyang Zheng, Luca Amendola, Valeria Pettorino, and Christof Wetterich, Early dark energy in the pre- and postrecombination epochs, Phys. Rev. D **104**, 083536 (2021).
[93] Michael S. Turner, Coherent scalar-field oscillations in an expanding universe, Phys. Rev. D **28**, 1243 (1983).
[94] Chung-Pei Ma and Edmund Bertschinger, Cosmological perturbation theory in the synchronous and conformal Newtonian gauges, Astrophys. J. **455**, 7 (1995).
[95] Thejs Brinckmann and Julien Lesgourgues, MontePython 3: Boosted MCMC sampler and other features, Phys. Dark Universe **24**, 100260 (2019).
[96] Benjamin Audren, Julien Lesgourgues, Karim Benabed, and Simon Prunet, Conservative constraints on early cosmology: An illustration of the Monte Python cosmological parameter inference code, J. Cosmol. Astropart. Phys. 02 (2013) 001.
[97] Julien Lesgourgues, The cosmic linear anisotropy solving system (CLASS) I: Overview, arXiv:1104.2932.
[98] Diego Blas, Julien Lesgourgues, and Thomas Tram, The cosmic linear anisotropy solving system (CLASS) II: Approximation schemes, J. Cosmol. Astropart. Phys. 07 (2011) 034.
[99] N. Aghanim *et al.* (Planck Collaboration), Planck 2018 results. V. CMB power spectra and likelihoods, Astron. Astrophys. **641**, A5 (2020).
[100] N. Aghanim *et al.* (Planck Collaboration), Planck 2018 results. VIII. Gravitational lensing, Astron. Astrophys. **641**, A8 (2020).
[101] Florian Beutler, Chris Blake, Matthew Colless, D. Heath Jones, Lister Staveley-Smith, Lachlan Campbell, Quentin Parker, Will Saunders, and Fred Watson, The 6dF galaxy survey: Baryon acoustic oscillations and the local Hubble constant, Mon. Not. R. Astron. Soc. **416**, 3017 (2011).
[102] Ashley J. Ross, Lado Samushia, Cullan Howlett, Will J. Percival, Angela Burden, and Marc Manera, The clustering of the SDSS DR7 main galaxy sample—I. A 4 per cent distance measure at $z = 0.15$, Mon. Not. R. Astron. Soc. **449**, 835 (2015).
[103] Héctor Gil-Marín *et al.*, The clustering of galaxies in the SDSS-III Baryon Oscillation Spectroscopic Survey: BAO measurement from the LOS-dependent power spectrum of

DR12 BOSS galaxies, Mon. Not. R. Astron. Soc. **460**, 4210 (2016).
[104] Francisco-Shu Kitaura *et al.*, The clustering of galaxies in the SDSS-III Baryon Oscillation Spectroscopic Survey: Mock galaxy catalogues for the BOSS Final Data Release, Mon. Not. R. Astron. Soc. **456**, 4156 (2016).
[105] Beth Reid *et al.*, SDSS-III Baryon Oscillation Spectroscopic Survey Data Release 12: Galaxy target selection and large scale structure catalogues, Mon. Not. R. Astron. Soc. **455**, 1553 (2016).
[106] Takahiro Nishimichi, Guido D'Amico, Mikhail M. Ivanov, Leonardo Senatore, Marko Simonović, Masahiro Takada, Matias Zaldarriaga, and Pierre Zhang, Blinded challenge for precision cosmology with large-scale structure: Results from effective field theory for the redshift-space galaxy power spectrum, Phys. Rev. D **102**, 123541 (2020).
[107] Ashley J. Ross *et al.*, The completed SDSS-IV extended Baryon Oscillation Spectroscopic Survey: Large-scale structure catalogues for cosmological analysis, Mon. Not. R. Astron. Soc. **498**, 2354 (2020).
[108] Chia-Hsun Chuang, Francisco-Shu Kitaura, Francisco Prada, Cheng Zhao, and Gustavo Yepes, EZmocks: Extending the Zel'dovich approximation to generate mock galaxy catalogues with accurate clustering statistics, Mon. Not. R. Astron. Soc. **446**, 2621 (2015).
[109] Florian Beutler and Patrick McDonald, Unified galaxy power spectrum measurements from 6dFGS, BOSS, and eBOSS, J. Cosmol. Astropart. Phys. 11 (2021) 031.
[110] Jiamin Hou *et al.*, The completed SDSS-IV extended Baryon Oscillation Spectroscopic Survey: BAO and RSD measurements from anisotropic clustering analysis of the quasar sample in configuration space between redshift 0.8 and 2.2, Mon. Not. R. Astron. Soc. **500**, 1201 (2020).
[111] D. M. Scolnic *et al.*, The complete light-curve sample of spectroscopically confirmed SNe Ia from Pan-STARRS1 and cosmological constraints from the combined Pantheon sample, Astrophys. J. **859**, 101 (2018).
[112] Alexander Mead, Samuel Brieden, Tilman Tröster, and Catherine Heymans, HMcode-2020: Improved modelling of non-linear cosmological power spectra with baryonic feedback, Mon. Not. R. Astron. Soc. **502**, 1401 (2021).
[113] Antony Lewis, GetDist: A Python package for analysing Monte Carlo samples, arXiv:1910.13970.
[114] Marco Raveri and Wayne Hu, Concordance and discordance in cosmology, Phys. Rev. D **99**, 043506 (2019).
[115] Adam G. Riess, Stefano Casertano, Wenlong Yuan, Lucas M. Macri, and Dan Scolnic, Large magellanic cloud Cepheid standards provide a 1% foundation for the determination of the Hubble constant and stronger evidence for physics beyond ΛCDM, Astrophys. J. **876**, 85 (2019).
[116] Elcio Abdalla *et al.*, Cosmology intertwined: A review of the particle physics, astrophysics, and cosmology associated with the cosmological tensions and anomalies, J. High Energy Astrophys. **34**, 49 (2022).
[117] Sunny Vagnozzi, Consistency tests of ΛCDM from the early integrated Sachs-Wolfe effect: Implications for early-time new physics and the Hubble tension, Phys. Rev. D **104**, 063524 (2021).
[118] Catherine Heymans *et al.*, KiDS-1000 cosmology: Multi-probe weak gravitational lensing and spectroscopic galaxy clustering constraints, Astron. Astrophys. **646**, A140 (2021).
[119] T. M. C. Abbott *et al.* (DES Collaboration), Dark Energy Survey Year 3 results: Cosmological constraints from galaxy clustering and weak lensing, Phys. Rev. D **105**, 023520 (2022).
[120] Gang Liu, Jiaze Gao, Yufen Han, Yuhao Mu, and Lixin Xu, Mitigating cosmological tensions via momentum-coupled dark sector model, Phys. Rev. D **109**, 103531 (2024).
[121] Guillermo Franco Abellán, Matteo Braglia, Mario Ballardini, Fabio Finelli, and Vivian Poulin, Probing early modification of gravity with Planck, ACT and SPT, J. Cosmol. Astropart. Phys. 12 (2023) 017.